Chapter 11
How Latitude Location on a Micro-World Enables Real-Time Nanoparticle Sizing

Steve Arnold, D. Keng, E. Treasurer, and M. R. Foreman

Abstract We have devised a method for using the nanoparticle induced frequency shift of whispering gallery modes (WGMs) in a microspheroid for the accurate determination of the nanoparticle size in real time. Before the introduction of this technique, size determination from the mode shift could only be obtained statistically based on the assumption that the largest perturbation occurs for binding at the equator. Determining the latitude of the binding event using two polar WGMs results in an analytic method for size determination using a single binding event. The analysis proceeds by incorporating the binding latitude into the *Reactive Sensing Principle* (*RSP*), itself containing a shape dependent form factor found using the Born approximation. By comparing this theory with experiments we find that our theoretical approach is more accurate than point dipole theory even though the optical size (circumference/wavelength) is considerably less than one.

11.1 Introduction

Our goal, since our last major advance reported at this school in 2013 [1], has been lofty: invent an accurate size spectrometer for nano-size particles that works in solution and in real-time. This is akin to a mass spectrometer that works in vacuum, and has acted as an enabler in biochemical discovery. Label-free sensors with these capabilities could identify whole viruses and exosomes not only by using bound antibodies [2, 3], but also through their size. Furthermore, a single particle technique with these capabilities could detect binding events in real-time and quantitatively test the efficacy of antibodies.

S. Arnold (✉) • D. Keng • E. Treasurer
Microparticle Photophysics Lab (MP3Lab), NYU School of Engineering, Brooklyn, NY 11201, USA
e-mail: sa1577@nyu.edu; sarnold935@aol.com

M.R. Foreman
Max Planck Institute for the Science of Light, Günther-Scharowsky-Straße 1, 91058 Erlangen, Germany

B. Di Bartolo et al. (eds.), *Nano-Optics: Principles Enabling Basic Research and Applications*, NATO Science for Peace and Security Series B: Physics and Biophysics, DOI 10.1007/978-94-024-0850-8_11

Since Arnold et al. first proposed microcavity based single nanoparticle detection and sizing in 2003, using the perturbative frequency/wavelength shift of an optical Whispering Gallery Mode (WGM), [4] there have been a slew of papers on the subject [5]. The mechanism invoked in Ref. [4], known as the Reactive Sensing Principle (*RSP*) [6] states that "the perturbation in a resonator's photonic energy upon particle binding is equal to the energy required for the microcavity's reactive (evanescent) field to polarize the particle". In 2010 Zhu et al. established a method for determining the size of a nanoparticle in one event by using an optical microresonator requiring a very high Q WGM resonator ($Q \sim 10^7$–10^8) and a combination of a reactive splitting $2G$, and an increase in linewidth $\Delta\Gamma$ associated with light scattering [7]. The splitting is caused by lifting the clockwise-counterclockwise degeneracy associated with orbiting photons within WGMs. Whereas the splitting is proportional to the polarizability α of the adsorbing nanoparticle, which is in turn proportional to the particle volume, the increase in linewidth is proportional to α^2, so that the ratio $\Delta\Gamma/(2G)$ can be used to obtain the polarizability, and from that the particle size/mass. The measurable splitting vanishes however, if it is smaller than the cavity linewidth, thereby setting a lower limit for the detectable nanoparticle size [8]. The resulting "degenerate" mode still shifts, but it is only possible to obtain the polarizability through a statistical approach. In particular, the largest wavelength shift in a distribution of many events can be analytically related to the particle size, since the maximum shift of the lowest order polar mode corresponds to binding directly at the equator [4]. Unfortunately because of the statistical nature of this approach one cannot be certain that the largest event in the distribution corresponds to a particle at the equator. Consequently the size obtained is uncertain and many events are needed to generate the distribution [9]. Fortunately, we found an alternative approach that avoids these difficulties [10]. Explaining how it works and its ramifications is the subject of this chapter.

11.2 The Way Forward

As mentioned above, the need for measurements of statistical ensembles to evaluate the particle size from the frequency/wavelength shift derives from the uncertainty in the binding particle's location. Accordingly, the only distinguishing feature in the ensemble is the largest shift, which occurs for a nanoparticle binding at the equator. Our new approach avoids these difficulties by determining where the particle binds. Because of the rotational symmetry associated with a spheroid, only determination of particle's latitude is necessary. Once the latitude is determined, the *RSP* can then be invoked for size determination. The current idea is fully reactive, does not require mode splitting, and therefore can be applied in the weak coupling limit where the interaction G is considerably smaller than the linewidth, Γ, and the Q is modest ($<10^6$). Nevertheless, like mode splitting it involves analysis of the ratio of shifts from two different resonances in the same microcavity and is therefore immune to long term temperature fluctuations. Specifically, this approach

involves the excitation of two resonances having the same angular momentum quantum number $\boldsymbol{l}$ but different m quantum numbers ($-l < m < l$) in a cavity for which a nanoparticle induced wavelength shift is much smaller than the linewidth (i.e. weak coupling). Although m is referred to as the magnetic quantum number in atomic physics, when considering different m modes within a microresonator for a given l we will use the term polar modes. To understand the principle of the latitude locator we must examine the shape of the WGM intensity of different polar modes. There are many such states that are characterized by $l - m + 1$ intensity peaks along the polar direction. In a sphere these m states are degenerate for a given angular momentum $\boldsymbol{l}$, but in a spheroid this degeneracy is lifted and the states separate spectrally. The first of these (i.e. shortest wavelength) is an equatorial mode for which $m = l$, thereby producing one intensity peak centered about the equator (Fig. 11.1). The next with $m = l - 1$, has two peaks, one to the North and the other to the South of the equator (Fig. 11.1). It is important to realize that the two modes depicted in Fig. 11.1 can be excited sequentially within the same slightly prolate microcavity by a fiber positioned slightly above or below the equator and directed along a line perpendicular to the symmetry axis of the spheroid. In what follows we will show that the ratio of the resonance wavelength shifts of each of these modes provides a measure of the nanoparticle's absolute latitude, from which its polarizability and size/mass may be estimated one event at a time (i.e. real time).

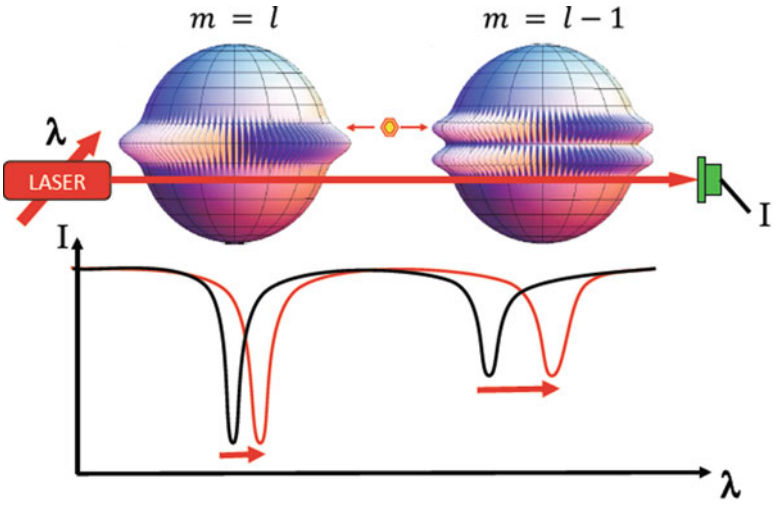

Fig. 11.1 Polar mode intensities in a single slightly prolate micro-spheroid excited sequentially during a spectral laser scan by a guided wave in a tapered fiber positioned just below the equator, and its corresponding transmission spectrum. The $m = l - 1$ mode on the *right* has a slightly longer resonance wavelength than the $m = l$ mode on the *left*. A nanoparticle adsorbed north of the equator (*orange dot*) has a larger overlap with the intensity of the $m = l - 1$ mode on the *right* and consequently this mode shifts (*red curve*) to a greater extent. The ratio of the two shifts for the same microcavity yields the nanoparticle's latitude, from which its polarizability and size/mass are calculated using the *Reactive Sensing Principle* (*RSP*)

11.3 Theoretical Approach

To start the description of the polar mode based locator we first update the wavelength shift theory to include differing polar modes. For this purpose we adopt the symbol $\Delta\lambda_{l,m}$ to describe the wavelength shift of a mode having an angular momentum number l, and polar number m. In what follows we will show that the latitude angle for particle binding is easily obtained from the ratio of two wavelength shifts, $\Delta\lambda_{l,l-1}/\Delta\lambda_{l,l}$.

To understand the importance of polar modes in nanoparticle characterization one simply has to return to the basic principle of microcavity reactive detection, the reactive sensing principle (*RSP*). To reiterate the *RSP* simply states that "the perturbation in a resonator's photonic energy upon particle binding is equal to the energy required for the microcavity's reactive (evanescent) field to polarize the particle" [4]. The principle applies to ultra-small particles such as proteins for which the radius a is much less than the characteristic evanescent intensity length L ($a<<$L), and to extended particles ($a\sim L$). On this basis, the shift in resonance wavelength $\Delta\lambda$ is the wavelength λ times the ratio of the energy required to polarize the nanoparticle to the energy in the cavity. In a dipole approximation ($a<<L$) the shift in wavelength is given by [4]

$$\Delta\lambda \simeq \frac{\alpha_{ex}\left|\boldsymbol{E}_0\left(\boldsymbol{r}_p\right)\right|^2}{2\int \varepsilon\left(r_c\right)\left|\boldsymbol{E}_0\left(\boldsymbol{r}_c\right)\right|^2 dV}\lambda, \tag{11.1}$$

where $\boldsymbol{E}_0(\boldsymbol{r}_\mathrm{p})$ is the evanescent field strength at the position of the dipole $\boldsymbol{r}_p$, α_ex is the polarizability of the nanoparticle in excess of it environment (i.e. medium), and $\varepsilon(\boldsymbol{r}_\mathrm{c})$ is the permittivity of the cavity at position $\boldsymbol{r}_\mathrm{c}$. When applied to a homogeneous microsphere for $m\approx \boldsymbol{l>>1}$ (i.e. polar modes whose mode energy is concentrated close to the equator), for a nanoparticle of radius a adsorbing on the surface, Eq. 11.1 becomes

$$\Delta\lambda_{l,m} \approx \frac{\alpha\left|Y_{l,m}\left(\xi_p\right)\right|^2 g\left(a/L\right)}{\left(n_s{}^2 - n_e{}^2\right)R_e{}^3}\lambda \tag{11.2}$$

where $\alpha = \alpha_{ex}/\varepsilon_0$ is the "geometric" polarizability that is proportional to the volume of the nanoparticle ($\alpha = D_\alpha a^3$), R_e is the microsphere equatorial radius, L is the characteristic evanescent intensity length obtained from Mie theory, $Y_{l,m}(\xi_\mathrm{p})$ is the spherical harmonic evaluated at the latitude ξ_p of the bound particle (the azimuthal dependence of the spherical harmonic is omitted since the usual $e^{im\phi}$ drops out when considering $|Y_{l,m}|$), the factor g can correct for a displacement of the point dipole from the surface (g_1), or for the more realistic case of a distributed polarization energy density (g_2), n_s, n_e and n_p are the refractive indices of the microsphere, environment and nanoparticle respectively, and finally the constant $D_\alpha = 4\pi n_e{}^2\left(n_p{}^2 - n_e{}^2\right)/\left(n_p{}^2 + 2n_e{}^2\right)$.

The simplest choice of the g factor, g_1, accounts for the displacement of the center of the dipole from the surface by a distance a. Since the evanescent intensity in the numerator of Eq. 11.1 fits well to a single exponential decay with a characteristic length L, [11] the simplest g factor is one that evaluates the evanescent intensity at the nanoparticle's center; [6]

$$g_1 = e^{-z} \tag{11.3}$$

where $z = a/L$. Alternatively we can use g_2, termed a form factor since it accounts for the shape of the nanoparticle, which can be found from making the Born approximation for scattering from a sphere [12]. Specifically, g_2 is the volume averaged surface normalized evanescent intensity within the nanoparticle. For a spherical nanoparticle, integration over its shape gives

$$g_2(z) = \frac{6}{(2z)^2}\left(1 + e^{-2z}\right) - \frac{12}{(2z)^3}\left(1 - e^{-2z}\right). \tag{11.4}$$

This form factor recognizes that the hemisphere of the nanoparticle closest to the microsphere surface will receive more polarization energy than the hemisphere furthest from the surface. Below $z \approx 1$, g_1 and g_2 are approximately equal and have the simple limiting value of $g \simeq 1$ for $a << \mathrm{L}$, therefore ensuring asymptotic consistency with the original result [4] (i.e. both describe the simple point dipole at the surface of the microcavity for $a << L$). The factor g_1 is expected to be valid so long as the ratio $X_\mathrm{n} = 2\pi \mathrm{a}/(\lambda/\mathrm{n_p}) < 1$, where λ is the free-space wavelength [13]. The limits for use of the form factor g_2 have become controversial, [13] although this paper will provide a test of its use in interpreting experimental data for z values both smaller and larger than 1. Equation 11.2 is the key to our latitude locator.

Consider the ratio of wavelength shifts of the $m = l - 1$ to the $m = l$ modes at a latitude ξ_p; $\Delta\lambda_{l,l-1}\left(\xi_p\right)/\Delta\lambda_{l,l}\left(\xi_p\right)$. So long as the shifts are very small in comparison to the wavelength and $l >> 1$, it follows from Eq. 11.2 that

$$\frac{\Delta\lambda_{l,l-1}}{\Delta\lambda_{l,l}} \cong \frac{\left|Y_{l,l-1}\left(\xi_p\right)\right|^2}{\left|Y_{l,l}\left(\xi_p\right)\right|^2}. \tag{11.5}$$

As one can see the right hand side of Eq. 11.5 only depends on the latitude ξ_p of the adsorbing particle, and consequently by placing experimental wavelength shift data on the left, this equation gives the latitude of the adsorbed nanoparticle independent of its physical properties, those of the resonator, or any refractive indices. Once ξ_p is determined, Eq. 11.2 can be used to calculate the size of the nanoparticle as well as the polarizability.

Our simple latitude locator equation (Eq. 11.5) can be further simplified by utilizing a mathematical identity which connects the ratio of spherical harmonics to the tangent of the latitude angle,

$$\frac{\Delta\lambda_{l,l-1}}{\Delta\lambda_{l,l}} \cong \left|\frac{Y_{l,l-1}\left(\xi_p\right)}{Y_{l,l}\left(\xi_p\right)}\right|^2 = 2l\,\left[\tan\left(\xi_p\right)\right]^2. \tag{11.6}$$

Combining Eq. 11.4 with Eq. 11.5 gives the absolute latitude of the particle,

$$\left|\xi_p\right| \cong \tan^{-1}\sqrt{\frac{1}{2l}\frac{\Delta\lambda_{l,l-1}}{\Delta\lambda_{l,l}}} \tag{11.7}$$

Once $|\xi_p|$ is found, the size a of the nanoparticle can be obtained by re-expressing Eq. 11.2 as

$$a^3 g\,(a/L) \approx \frac{\left(n_s{}^2 - n_e{}^2\right)R^3}{\left|Y_{l,l}\left(\xi_p\right)\right|^2 D_\alpha}\frac{\Delta\lambda_{l,l}}{\lambda}. \tag{11.8}$$

The solution to Eq. 11.8 is particularly simple for $a << L$ since the form factor $g \simeq 1$ in this limit, and one gets a closed form algebraic solution. For ultra-small particles displaced from the surface, or larger particles for which the evanescent field varies significantly over the dielectric body, g can take an analytical form (e.g. g_1 or g_2), and the size can be obtained numerically from Eq. 11.8. Whether the nanoparticle is north or south of the equator is irrelevant, since the square modulus of the spherical harmonic in the denominator of Eq. 11.8 is an even function with respect to the latitude.

11.4 Experimental Approach

To test our micro-global latitude locator idea we fabricated micro-spheroids by using CO_2 laser melting at the end of a tapered silica optical fiber (inset, Fig. 11.2). Shape analysis of the images revealed that our resonators were slightly prolate [distortion $= \left(R_p - R_e\right)/\left(R_p R_e^2\right)^{1/3} < 0.03$, where R_p is the polar radius and R_e is that of the equator]. These silica micro-spheroids were then installed into our homemade microfluidic system, [2, 14, 15] where they were coupled to a tapered optical fiber. In the inset the fiber is below the equator of the spheroid.

A typical under-coupled spectrum taken through the coupling fiber is shown in Fig. 11.2. All of the resonances were excited with a 1063 nm tunable DFB laser polarized along a meridian [Transverse Electric (TE) polarization] by using an integrated system provided by MP3Laser.com. The laser was current tuned with a saw tooth wave that accounts for the rising backbone of the spectrum; increasing the drive current tunes the laser to greater wavelength but also increases its output power. It should be noted that the resonance dip on the left has no neighbor at shorter wavelength. This is the signature of the $m = l$ equatorial mode of a prolate spheroid; the $m = l$ mode has the shortest wavelength, since the equator has the smallest circumference [16]. To the right of this mode (longer wavelength) is the $m = l - 1$ mode which is narrower with a smaller dip. Note that the $m = l - 2$ mode is of similar depth to the $m = l$ mode, while the $m = l - 3$ mode (at yet longer wavelength) looks similar in depth to the $m = l - 1$ mode. This sequence of deep-

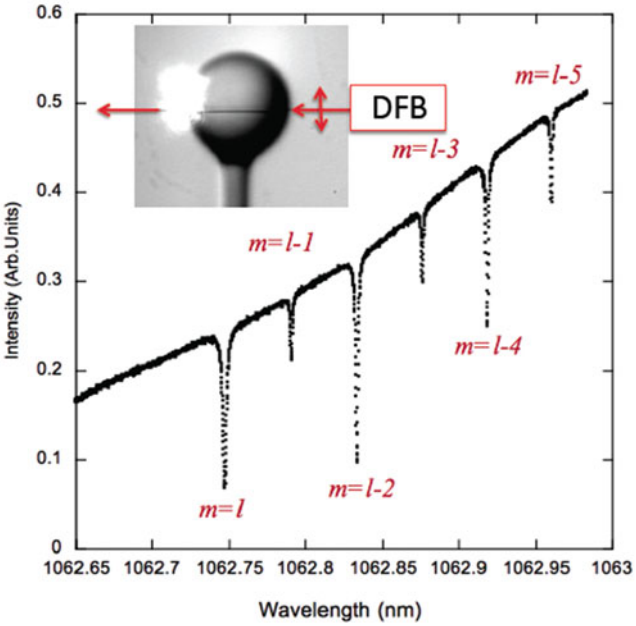

Fig. 11.2 Spectrum of a slightly prolate microcavity immersed in 30 mM NaCl solution and excited by tapered fiber coupling just below the equator as seen in the *inset*. The equatorial radius was 41 microns. From Mie theory $l = 340$ with all modes having TE polarization. The DFB laser was scanned with a saw tooth drive having a period of 100 msec

shallow-deep-shallow dips in Fig. 11.2 is a consequence of the overlap between the fiber field and the polar symmetries of the WGMs; the coupling constant requires performing volume integration over the product of the optical fiber field with the WGM field [17]. Whereas the $m = l$ mode is symmetric in latitude about the equator as is the fiber field, the $m = l - 1$ mode is antisymmetric. Exciting the antisymmetric WGM mode requires that the centerline of the exciting fiber be slightly above or below the equator due to the greater modal overlap this gives. Before performing nanoparticle binding experiments the fiber contacted the cavity which reduced noise due to fiber vibration, but caused the resonances to be both red shifted and broadened due to over-coupling. All the modes were identified as being of first radial order.

The latitude locator idea was tested by using nanoparticles for which $X_n < 1$. For convenience polystyrene beads were chosen with a manufactured size of $\langle a_m \rangle \pm \sigma_m = 96.7 \pm 4.5$ nm [Polysciences], for which $X_\mathrm{n} = 0.90$ at 1063 nm. These particles were injected into our microfluidic system at a 175 fM concentration in the presence of a resonator similar to that depicted in Fig. 11.2, but with an equatorial radius of 40.5 μm. The solution had a 100 mM NaCl concentration to promote binding to the silica surface by decreasing the Debye length associated with ionized silanol groups [6]. The fiber is placed in contact with the resonator to reduce mechanical vibration

Table 11.1 Data (*2nd and 3rd column*) taken for polystyrene particles with a size of $\langle a_m \rangle \pm \sigma_m = 96.7 \pm 4.5$ nm, as determined by the manufacturer. The mean size found using our latitude locator scheme differs from $\langle a_m \rangle$ by 1.3 % when using g_1, and by 0.4 % when using g_2. The common parameters used to calculate columns 5 and 6 are $R = 40.5$ μm, $l = 336$, $L = 194.4$, $n_p = 1.5718$, $n_s = 1.449$ and $n_e = 1.326$

Event		$\Delta\lambda_{336,336}$ (*fm*)	$\Delta\lambda_{336,335}$ (*fm*)	$\lvert\xi_p\rvert$ (deg) Eq. 11.7	$a_{rsp}(nm)$ Eq. 11.8, g_1	$a_{rsp}(nm)$ Eq. 11.8, g_2
1.	90 s	100	58	1.69	103.9	102.8
2.	130 s	120	18	0.86	102.6	101.4
3.	485 s	37	74	3.13	92.7	91.9
4.	1358 s	25	85	4.08	104.7	103.6
5.	1612 s	38	66	2.92	88.9	88.2
6.	2601 s	63	68	2.30	95.4	94.5
7.	4038 s	45	75	2.86	93.8	92.9
8.	4412 s	110	51	1.51	105.5	104.3
9.	4917 s	64	83	2.52	100.3	99.2
10.	5225 s	64	55	2.05	91.9	91.1
11.	6863 s	62	79	2.50	98.6	97.6
12.	7182 s	58	73	2.48	95.7	94.8
13.	7310 s	73	77	2.27	100.7	99.7
Mean					**98.0**	**97.1**
$< a_{rsp} > - < a_m >$					**1.3**	**0.4**

noise. This results in a red shift and broadening of the resonances. Upon coupling the $m = l$ and $m = l - 1$ resonances had Qs of 5×10^5 and 2×10^5, respectively.

The second and third columns of Table 11.1 show the experimental shifts for 13 detected events, measured over a period in excess of 2 h, while the fourth column provides the latitude angle found from Eq. 11.7. The fifth and sixth columns provide the nanoparticle size determined from Eq. 11.8 using form factors g_1 or g_2, respectively. As one can see the mean radius determined using the *RSP* for both g_1 (98.0 nm) and g_2 (97.1 nm) are near the manufacturer's specified size, although the mean radius using g_2 is considerably closer to the manufacturer's value of 96.7 nm.

The standard deviation of all the particle results determined using Eq. 11.8 (5.0 nm) is very close to the manufacturer's standard deviation of 4.5 nm, implying that our standard deviation is the result of particle size variation, and not the computational approach.

11.5 Concluding Remarks

For the data in Table 11.1 $X_n = 0.9$, which easily qualifies for testing our sizing technique based on g_1, [13] however it appears that g_2 provides better agreement with our data. The mean size arrived at using our global positioning scheme differs

from $\langle a_m \rangle$ by deviations of about +1.3 % using g_1, and by + 0.4 % using g_2. It is not difficult to understand the superiority of g_2 over g_1.

Reference [13] suggests that the intensity in the numerator of Eq. 11.1 should be evaluated at the center of the nanoparticle so long as $X_n < 1$. The upper limit in size consistent with this inequality is $a_{max} = \lambda/(2\pi n_p)$, which for polystyrene particles at 1063 nm is about 108 nm. For the microcavity used in Table 11.1, $L = 194.4$ nm, so the intensity at the furthest part of the bound nanoparticle is only 33 % of what it is at the microcavity surface. This is expected to lead to a decidedly inhomogeneous energy density within the particle. In other words the centroid of energy density within the particle cannot be at the center as it would be for a uniform intensity; **considering the current high precision of our measurements, a point dipole model is less reasonable than the shape dependent Born approximation even for $X_n < 1$.**

To further support our conclusion a COMSOL simulation was performed for microcavity and nanoparticle parameters similar to those in Table 11.1. Figure 11.3 shows a typical calculation. The intensity within the particle falls off by a factor of 2.87 from the closest point to the microcavity to the furthest point even though X_n <1. This image allows us to calculate the total polarization energy of the particle. The results are consistent with the *RSP* theory for a non-uniform polarization density, [18] and with the use of the form factor g_2 [19].

Whereas the factor g_1 requires that the particle be viewed as a displaced dipole having $X_n < 1$, [13] the limitation on the Born approximation as applied to polarization by an transverse electric (TE) evanescent field is not as apparent. To test this we increased the particle size so that X_n reached 2.1, by performing experiments on polystyrene particles having mean radii of 178 nm and 228 nm [19]. Surprisingly, when using g_2 the results were nearly as good as those for the smaller particles in Table 11.1; with the measured mean radii deviating from the manufacturer specified means of 178 nm and 228 nm by +0.5 % and +0.8 % respectively. By comparison the displaced point dipole factor g_1 does not compare well as expected; the mean radii calculated with g_1 deviate away from the manufacturer specified means of 178 nm and 228 nm by +3.6 % and +8.9 % respectively; ∼10 × the deviation encountered by using g_2.

We have just begun our work on constructing high precision nanoparticle size measurements in real time. One thing which is quite clear from our measurements and simulations is that the dipole theory even in a "first principled" form [13] is not sufficient, and that perturbation theory can prove more accurate because it allows for variation in the internal field.

At its inception we called the technique to locate the nanoparticle's binding site, a micro-global positioning system (WGM-gps) [10]. Ordinarily a global positioning system needs to report latitude, longitude and altitude, however it would seem from Table 11.1 that we only located the latitude. In point of fact by identifying the particle's size we have determined the "altitude" to its center at its landing site. Consequently a pre-binding record of the frequency shift by a single particle can determine its "altitude" history before and at the time of landing. In that sense we can have both the latitude and altitude. Although not necessary for particle

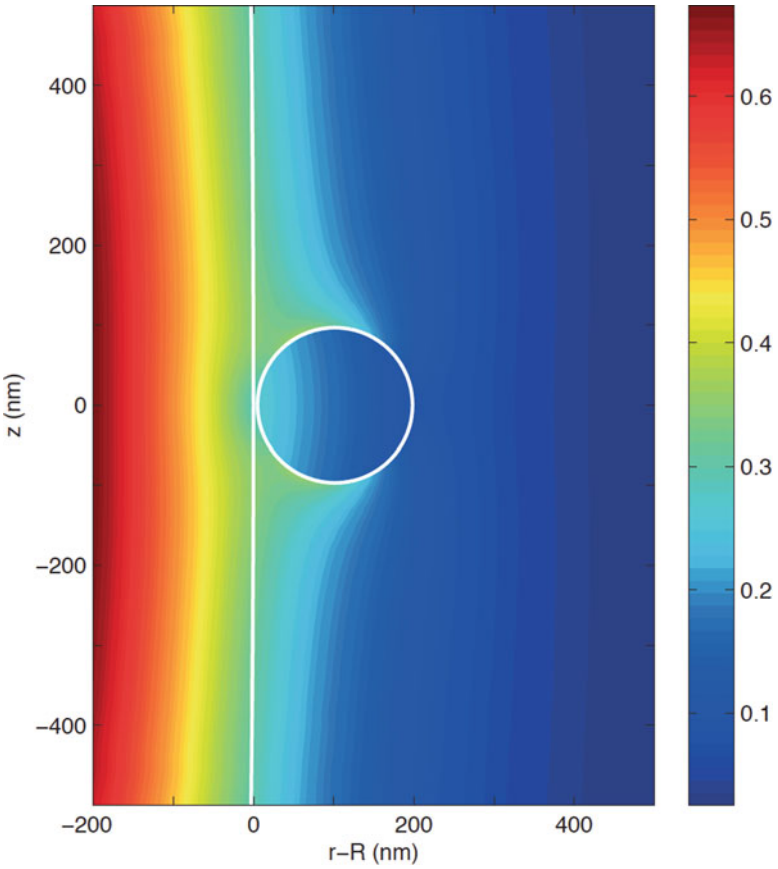

Fig. 11.3 COMSOL calculation showing the internal field within a 96.7 nm radius polystyrene particle located at the equator of a spheroidal resonator and bathed in a TE field of a 1st order WGM with $l = 340$. The position of the *vertical white line* closest to the nanoparticle represents the surface of the microcavity. The intensity within the particle falls off by a factor of 2.87 from the closest point to the microcavity to the furthest point even though $X_n < 1$

sizing, the determination of longitude would complete our WGM-gps sensor leading to massive multiplexing by comparison to the manner in which WGM sensors are currently used (i.e. one assay per resonator). This should revolutionize sensor technology on our micro-world, just as it revolutionized navigation on the Earth centuries ago [19].

Acknowledgements The research described herein was supported by the National Science Foundation grant EECS 1303499.

References

1. Arnold, S., Holler, S., & Fan, X. (2015). Taking microcavity label-free single molecule detection deep into the protein realm: Cancer marker detection at the ultimate sensitivity. In *Nano-structures for optics and photonics* (pp. 309–322). Dordrecht: Springer.
2. Arnold, S., Ramjit, R., Keng, D., Kolchenko, V., & Teraoka, I. (2008). Microparticle photophysics illuminates viral bio-sensing. *Faraday Discussions, 137*, 65–83.
3. McClellan, M. S., Domier, L. L., & Bailey, R. C. (2012). Label-free virus detection using silicon photonic microring resonators. *Biosensors and Bioelectronics, 31*, 388–392.
4. Arnold, S., Khoshsima, M., Teraoka, I., Holler, S., & Vollmer, F. (2003). Shift of whispering-gallery modes in microspheres by protein adsorption. *Optics Letters, 28*, 272–274.
5. Foreman, M. R., Swaim, J. D., & Vollmer, F. (2015). Whispering gallery mode sensors. *Advances in Optics and Photonics, 7*, 168–240.
6. Arnold, S., Keng, D., Shopova, S. I., Holler, S., Zurawsky, W., & Vollmer, F. (2009). Whispering gallery mode carousel. *Optics Express, 17*, 6230–6238.
7. Zhu, J., Ozdemir, S. K., Xiao, Y. F., Li, L., He, L., Chen, D. R., & Yang, L. (2010). On-chip single nanoparticle detection and sizing by mode splitting in an ultrahigh-Q microresonator. *Nature Photonics, 4*, 46–49.
8. Kim, W., Özdemir, Ş. K., Zhu, J., & Yang, L. (2011). Observation and characterization of mode splitting in microsphere resonators in aquatic environment. *Applied Physics Letters, 98*, 141106.
9. Lu, T., Lee, H., Chen, T., Herchak, S., Kim, J. H., Fraser, S. E., Flagan, R., & Vahala, K. (2011). High sensitivity nanoparticle detection using optical microcavities. *Proceedings of the National Academy of Sciences, 108*, 5976–5979.
10. Keng, D., Tan, X., & Arnold, S. (2014). Whispering gallery micro-global positioning system for nanoparticle sizing in real time. *Applied Physics Letters, 105*, 071105.
11. Khoshsima, M. (2004). *Perturbation of whispering gallery modes in microspheres by protein adsorption: Theory and experiment*. Doctoral dissertation, Polytechnic University.
12. Vollmer, F. (2004). *Resonant detection of nano to microscopic objects using whispering gallery modes*. Doctoral dissertation, The Rockefeller University.
13. Deych, L., & Shuvayev, V. (2015). Spectral modification of whispering-gallery-mode resonances in spheroidal resonators due to interaction with ultra-small particles. *Optics Letters, 40*, 4536–4539.
14. Keng, T. K. D. (2009). *Whispering gallery mode bioparticle sensing and transport*. Doctoral dissertation, Polytechnic Institute of New York University.
15. Keng, D., McAnanama, S. R., Teraoka, I., & Arnold, S. (2007). Resonance fluctuations of a whispering gallery mode biosensor by particles undergoing Brownian motion. *Applied Physics Letters, 91*, 103902.
16. Lin, G., Qian, B., Oručević, F., Candela, Y., Jager, J. B., Cai, Z., Lefevre-Segun, V., & Hare, J. (2010). Excitation mapping of whispering gallery modes in silica microcavities. *Optics Letters, 35*, 583–585.
17. Little, B. E., Laine, J. P., & Haus, H. A. (1999). Analytic theory of coupling from tapered fibers and half-blocks into microsphere resonators. *Journal of Lightwave Technology, 17*, 704–715.
18. Teraoka, I., & Arnold, S. (2006). Theory of resonance shifts in TE and TM whispering gallery modes by nonradial perturbations for sensing applications. *Journal of the Optical Society of America B, 23*, 1381–1389.
19. Sobel, D. (2007). *Longitude: The true story of a lone genius who solved the greatest scientific problem of his time*. New York: Bloomsbury Publishing.